PHYSICAL REVIEW B **89**, 165130 (2014)

GW calculations on post-transition-metal oxides

Youngho Kang,[1] Gijae Kang,[1] Ho-Hyun Nahm,[2,3] Seong-Ho Cho,[4] Young Soo Park,[4] and Seungwu Han[1,*]

[1]*Department of Materials Science and Engineering and Research Institute of Advanced Materials, Seoul National University, Seoul 151-755, Korea*

[2]*Center for Correlated Electron Systems, Institute for Basic Science (IBS), Seoul 151-747, Korea*

[3]*Department of Physics and Astronomy, Seoul National University, Seoul 151-747, Korea*

[4]*Compound Semiconductor Laboratory, Samsung Advanced Institute of Technology, Samsung Electronics Corporation, Yongin-Si, Gyeonggi-Do 446-712, Korea*

(Received 13 January 2014; revised manuscript received 19 March 2014; published 23 April 2014)

In order to establish the reliable *GW* scheme that can be consistently applied to post-transition-metal oxides (post-TMOs), we carry out comprehensive *GW* calculations on electronic structures of ZnO, Ga_2O_3, In_2O_3, and SnO_2, the four representative post-TMOs. Various levels of self-consistency (G_0W_0, GW_0, and $QPGW_0$) and different starting functionals (GGA, GGA + U, and hybrid functional) are tested and their influence on the resulting electronic structure is closely analyzed. It is found that the GW_0 scheme with GGA + U as the initial functional turns out to give the best agreement with experiment, implying that describing the position of metal-*d* level precisely in the ground state plays a critical role for the accurate dielectric property and quasiparticle band gap. Nevertheless, the computation on ZnO still suffers from the shallow Zn-*d* level and we propose a modified approach ($GW_0 + U_d$) that additionally considers an effective Hubbard U term during GW_0 iterations and thereby significantly improves the band gap. It is also shown that a GGA + U-based $GW_0(+U_d)$ scheme produces an accurate energy gap of crystalline $InGaZnO_4$, implying that this can serve as a standard scheme that can be applied to general structures of post-TMOs.

DOI: 10.1103/PhysRevB.89.165130 PACS number(s): 71.15.−m, 71.20.Nr, 81.05.Hd

I. INTRODUCTION

Post-transition-metal oxides (post-TMOs) such as ZnO, Ga_2O_3, In_2O_3, and SnO_2 are key materials in various optical, electrical, and energy devices owing to a unique combination of material properties, i.e., metallic conductivity and optical transparency. They share the same d^{10} configuration and highly dispersive conduction bands. Recently, transparent semiconducting oxides such as In-Ga-Zn-O are attracting a good deal of attention due to the application to thin-film transistors in the next-generation display, spurring theoretical and experimental researches on compound structures of post-TMOs [1–3].

On the theoretical side, the density-functional theory (DFT) within the local-density approximation (LDA) or generalized-gradient approximation (GGA) has been extensively employed for investigating various electronic properties of post-TMOs. However, the band-gap underestimation by DFT, which originates from the lack of derivative discontinuity and spurious self-interaction, has been particularly acute in post-TMOs. For instance, the LDA or GGA energy gap of ZnO is only 0.6–0.8 eV [4,5] in comparison with the experimental value of 3.44 eV [6], which corresponds to ∼80% underestimation. For other post-TMOs, the error ranges over 50%–70% [7,8], which is more serious than 30%–40% underestimation in typical insulators [9]. This is a critical issue in the theoretical study of these materials [10] because they are widely used in optoelectronic applications and so the band gap is a key parameter. In addition, it is difficult to make a clear interpretation of computational results when they are related to the band gap, for instance, defect formation energies [11]. It is well known that the severe band-gap underestimation is deeply related to the energetic position of the semicore metal-*d* band which is close to the valence band and leads to significant interaction with the oxygen-*p* band [12,13].

The band-gap underestimation in post-TMOs could be addressed in part by LDA(GGA) + U [12,14]. In this method, the metal-*d* bands are lowered in energy by the orbital-dependent on-site energy (U), which concurrently pulls down the oxygen *p* bands and increases the band gap. However, we note that +U methods tend to reduce the lattice parameters as well, and this also contributes to widening the band gap. For example, the band gap in Ga_2O_3 expands by only 0.26 eV if +U is applied with the lattice parameters fixed to GGA values. However, the gap increases by 1 eV when only the lattice parameters are adjusted from GGA to GGA + U values. Therefore, the energy-gap improvement by +U methods is partly accidental. Alternatively, the hybrid functional scheme incorporating the Hartree-Fock approximation is used to improve the band gap [15,16]. However, the fraction of the exact exchange energy should be varied among post-TMOs to fit the energy gap (ZnO: 37%, Ga_2O_3: 35%, In_2O_3: 29%, and SnO_2: 33% from our study) and this could be problematic in calculating compound structures.

Recently, the many-body perturbation theory within the *GW* approximation has begun to be widely used as it provides the quaisparticle band structure in a nonempirical way [6,17]. As such, several studies have been devoted to *GW* calculations on post-TMOs but they are mostly limited to a one-shot G_0W_0 scheme based on the DFT results [18–23] except for ZnO in which various levels of *GW* methods were tested [6,24–27]. Considering that the self-consistency is important to improve the agreement with experiment [6], extensive *GW* calculations on post-TMOs are essential to appreciate the full accuracy of *GW* methods in this class of materials. (Various levels

*hansw@snu.ac.kr

of self-consistency in GW calculations will be explained in the next section.) In this article, therefore, we systematically apply GW approaches to ZnO, Ga_2O_3, In_2O_3, and SnO_2, the four representative post-TMOs, and examine the effect of self-consistency and initial DFT functionals. We find that the GW_0 scheme with the dielectric matrix fixed to the GGA + U result, consistently produces the best agreement with experiment. For ZnO, however, the d electrons are still underbound and we propose a modified GW scheme to resolve this problem. The rest of the paper is organized as follows: in Sec. II we overview GW methods and provide computational details. The main results are presented and discussed in Secs. III A–III C. The results of the alternative method of quasiparticle calculation based on Coulomb-hole plus screened exchange (COHSEX) approximation is discussed in Sec. III D. The influence of pseudopotential type is discussed in Sec. III E. The results on a quaternary post-TMOs is provided in Sec. III F. Finally, we summarize and conclude in Sec. IV.

II. COMPUTATIONAL METHODS

A. Overview of GW approximation

In this subsection we will briefly overview GW methods and explain various levels of self-consistency. For more detailed information we refer to Ref. [28]. In GW approximation, the quasiparticle energy ($\epsilon_{n\mathbf{k}}$) for the nth band with the Bloch-vector $\mathbf{k}$ is determined perturbatively based on the DFT results:

$$\epsilon_{n\mathbf{k}} = \mathrm{Re}[\langle\psi_{n\mathbf{k}}|T + V_{\mathrm{ion}} + V_H + \Sigma(\epsilon_{n\mathbf{k}})|\psi_{n\mathbf{k}}\rangle], \quad (1)$$

where T is the kinetic energy operator, V_{ion} is the ionic potential, V_H is the Hartree potential, and Σ is the self-energy operator. For the update of the quasiparticle energies in Eq. (1), the linearization scheme based on the Newton-Raphson method is employed considering the renormalization factor explicitly. In the GW approximation, the nonlocal and energy-dependent operator Σ is described as follows:

$$\Sigma(\mathbf{r},\mathbf{r}',\epsilon) = \frac{i}{4\pi}\int_{-\infty}^{\infty} e^{i\omega'\delta} G(\mathbf{r},\mathbf{r}',\epsilon+\omega')W(\mathbf{r},\mathbf{r}',\omega')d\omega', \quad (2)$$

where G is the Green's function, W is the screened Coulomb interaction, and δ is an infinitesimal. Then, the self-energy term in Eq. (1) can be evaluated in the reciprocal space:

$$\Sigma(\epsilon)_{n\mathbf{k},n\mathbf{k}} = \frac{1}{\Omega}\sum_{\mathbf{q}\mathbf{G}\mathbf{G}'}\sum_{n'}\frac{i}{2\pi}\int_{-\infty}^{\infty} d\omega' W(\mathbf{G}+\mathbf{q},\mathbf{G}'+\mathbf{q},\omega') \times \langle\psi_{n\mathbf{k}}|e^{i(\mathbf{q}+\mathbf{G})\mathbf{r}}|\psi_{n'\mathbf{k}-\mathbf{q}}\rangle\langle\psi_{n'\mathbf{k}-\mathbf{q}}|e^{-i(\mathbf{q}+\mathbf{G}')\mathbf{r}'}|\psi_{n\mathbf{k}}\rangle \times \frac{1}{\epsilon+\omega'-\epsilon_{n'\mathbf{k}-\mathbf{q}}+i\eta\,\mathrm{sgn}[\epsilon_{n'\mathbf{k}-\mathbf{q}}-\mu]}, \quad (3)$$

where Ω is the cell volume, $\mathbf{q}$ and $\mathbf{G}$ are Bloch and reciprocal lattice vectors, respectively, η is an infinitesimal broadening factor, and μ is the Fermi energy.

The screened Coulomb interaction W is the product of the bare Coulomb kernel and the inverse dielectric matrix (ε^{-1}):

$$W(\mathbf{G}+\mathbf{q},\mathbf{G}'+\mathbf{q},\omega) = 4\pi e^2\frac{1}{|\mathbf{q}+\mathbf{G}|}\varepsilon_{\mathbf{q}}^{-1}(\mathbf{G},\mathbf{G}',\omega)\frac{1}{|\mathbf{q}+\mathbf{G}'|}. \quad (4)$$

The dynamical dielectric matrix in Eq. (4) can be evaluated in random-phase approximation (RPA) [29]:

$$\varepsilon_{\mathbf{q}}(\mathbf{G},\mathbf{G}',\omega) = \delta_{\mathbf{G},\mathbf{G}'} - \frac{4\pi e^2}{|\mathbf{q}+\mathbf{G}||\mathbf{q}+\mathbf{G}'|}\chi_{\mathbf{q}}^0(\mathbf{G},\mathbf{G}',\omega), \quad (5)$$

$$\chi_{\mathbf{q}}^0(\mathbf{G},\mathbf{G}',\omega) = \frac{1}{\Omega}\sum_{n,n',\mathbf{k}} 2w_{\mathbf{k}}(f_{n'\mathbf{k}-\mathbf{q}} - f_{n\mathbf{k}}) \times \frac{\langle\psi_{n'\mathbf{k}-\mathbf{q}}|e^{-i(\mathbf{q}+\mathbf{G})\mathbf{r}}|\psi_{n\mathbf{k}}\rangle\langle\psi_{n\mathbf{k}}|e^{-i(\mathbf{q}+\mathbf{G}')\mathbf{r}'}|\psi_{n'\mathbf{k}-\mathbf{q}}\rangle}{\omega+\epsilon_{n'\mathbf{k}-\mathbf{q}}-\epsilon_{n\mathbf{k}}+i\eta\,\mathrm{sgn}[\epsilon_{n'\mathbf{k}-\mathbf{q}}-\epsilon_{n\mathbf{k}}]}, \quad (6)$$

where $\chi_{\mathbf{q}}^0$ is the independent-particle polarizability, $w_{\mathbf{k}}$ is the $\mathbf{k}$-point weight, and $f_{n\mathbf{k}}$ represents the occupancy of the given one-electron state. As shown in Eqs. (2)–(6), the evaluation of self-energy requires the wave functions ($\psi_{n\mathbf{k}}$) and eigenvalues ($\epsilon_{n\mathbf{k}}$). If they are fixed to DFT results, it is called the single-shot G_0W_0 calculation and this does not require any iteration. One can also impose self-consistency in G and/or W such that $\epsilon_{n\mathbf{k}}$ appearing in Eqs. (3) and (6) correspond to quasiparticle energies in Eq. (1). This brings forth GW_0 and GW schemes. In $QPGW_0$ or $QPGW$, finally, the wave functions are updated together with eigenvalues by applying a Hermitian approximation to Σ [6].

B. Computational setup

All computations in this work were carried out using the Vienna *ab initio* simulation package (VASP) [30]. The ionic potentials are of the projector-augmented wave (PAW) [31] type and the semicore d electrons of metals are included as valence electrons. The energy cutoff of 500 eV is used for the plane-wave basis set. The crystal phases we examined are wurtzite ZnO, β-Ga_2O_3, cubic In_2O_3, and rutile SnO_2. (See Fig. 1.) For the response function χ^0 in Eq. (6), the energy cutoff of 250 eV is used. It was demonstrated that GW results critically depend on the computational parameters such as the $\mathbf{k}$-point density and the number of virtual states in the band summation [32]. To test the convergence with respect to these parameters, we carried out test G_0W_0 calculations for each

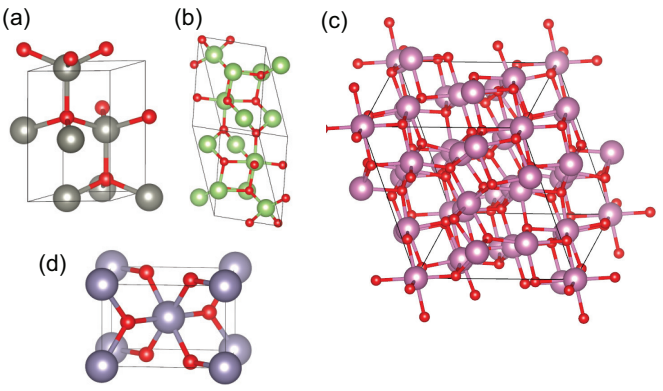

FIG. 1. (Color online) The primitive cells of (a) wurtzite ZnO, (b) β-Ga_2O_3, (c) cubic In_2O_3, and (d) rutile SnO_2. The red (small) balls in each crystal indicates oxygen and other larger ones are metal atoms.

material. The selected parameters are $9 \times 9 \times 7$ (ZnO), $4 \times 4 \times 4$ (Ga_2O_3), $3 \times 3 \times 3$ (In_2O_3), and $5 \times 5 \times 7$ (SnO_2) for the Γ-centered **k**-point mesh and 160 (ZnO), 120 (Ga_2O_3), 576 (In_2O_3), and 160 (SnO_2) bands for the band summation. This set of parameters ensure the convergence of the quasiparticle gap within 0.1 eV.

For the starting DFT calculations, we employ three kinds of exchange-correlation functionals: PBE-based GGA [33], GGA + U [34], and HSE06 hybrid functionals [35]. The effective U (U_{eff}) values applied on metal d orbitals are chosen to match with the experimental d-band positions [12]. For the fair comparison, we consistently use the experimental lattice parameters [19,36] since the energy gap is sensitive to the lattice parameter as mentioned in the Introduction. The internal atomic positions were relaxed with the PBE functional. For HSE06 calculations, we fix the fraction of the exact-exchange term to 0.25. The frequency-dependent inverse dielectric matrix in Eq. (4) is considered by including local field effects in passing from Eq. (5) to Eq. (4).

III. RESULTS AND DISCUSSION

A. Choice of W_0 and quasiparticle energy gap

In this study we mainly rely on the W_0 scheme in which the dielectric matrix is fixed to that determined before the GW iteration. This is because the errors from RPA and small band gap in DFT systematically cancel each other, thereby producing macroscopic optical dielectric constants ($\varepsilon^{\infty}_{\text{RPA}}$) close to the experimental reference values [28]. This means that if eigenvalues in W are updated with quasiparticle levels, the dielectric response is underestimated, resulting in the overestimation of the band gap. Therefore, we mainly compare G_0W_0, GW_0, and $QPGW_0$ results.

To choose an appropriate ground state DFT functional that specifies W_0, we examine $\varepsilon^{\infty}_{\text{RPA}}$ based on GGA, GGA + U, and HSE06 (see Fig. 2). As mentioned above, RPA tends to underestimate the dielectric response. Therefore, in spite of the underestimation of the band gap, $\varepsilon^{\infty}_{\text{RPA}}$ of GGA and GGA + U show good agreements with experimental data mostly, whereas HSE06 underestimates ε^{∞} due to larger band gaps. It is also seen that $\varepsilon^{\infty}_{\text{RPA}}$ based on GGA + U is improved over that from GGA for all tested materials. In particular, a significant improvement is noticeable for ZnO. This is because the d level in ZnO is close to the valence band and the band gap is overly underestimated in conventional DFT. In consideration of $\varepsilon^{\infty}_{\text{RPA}}$, therefore, GGA + U is chosen as the starting DFT functional for the following GW_0 calculations.

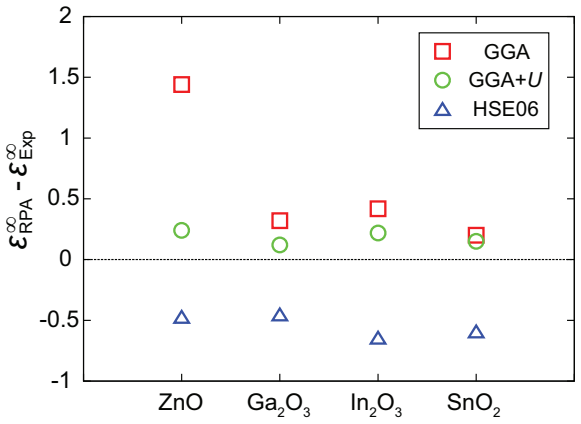

FIG. 2. (Color online) (Color online). Difference between theoretical and experimental macroscopic optical dielectric constant $\varepsilon^{\infty}_{\text{RPA}}$ and $\varepsilon^{\infty}_{\text{Expt.}}$, respectively. Except for In_2O_3, optical constants are anisotropic, and so we averaged diagonal components of the dielectric tensor. The experimental values are 3.73, 3.57, 4.00, and 3.92 for ZnO [37], Ga_2O_3 [38], In_2O_3 [20], and SnO_2 [17], respectively.

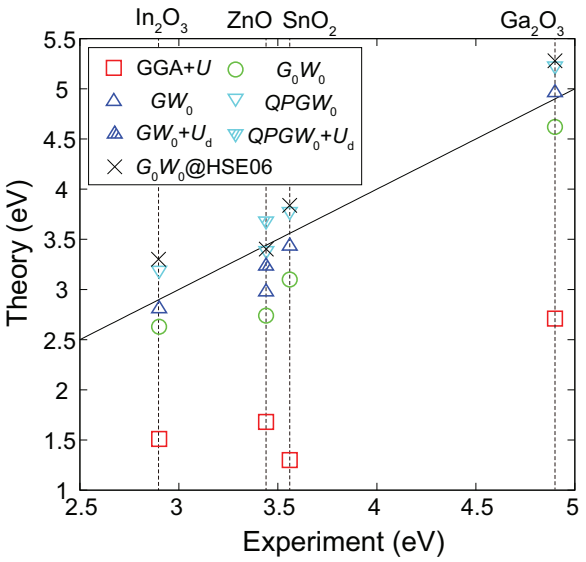

FIG. 3. (Color online) The band gaps computed with various computational schemes are plotted with respect to experimental values. See Table I for the numerical values.

In Fig. 3 we present the quasiparticle band gaps computed with various levels of GW approximations. Numerical values are compiled in Table I. The experimental band gaps for Ga_2O_3 and In_2O_3 were measured by photoemission spectroscopy, and therefore they are directly comparable with the computed quasiparticle band gaps. In the case of ZnO and SnO_2, the gap was obtained from two-photon absorption experiments, and so the exciton binding energies of 60 meV (ZnO) [39] and 30 meV (SnO_2) [40] could be considered for the accurate comparison between GW and experimental band gaps, but we neglect this in this work. In Fig. 3 the theoretical gap is presented against the experimental gap and the solid line indicates the perfect agreement with experiment. The band gaps from GGA + U calculations are also displayed as squares, which shows that the energy gap is severely underestimated. In contrast, it is found that G_0W_0 (circles) significantly improves the band gap with the mean absolute residual error (MARE) of 12.33%. However, a systematic underestimation of the band gap still persists. When the eigenvalues are updated in GW_0, the agreement with experimental values becomes closer and the resulting MARE is 5.49%. The only exception is ZnO and this is due to the underbinding of the Zn-d level as will be clarified below. When the wave functions are also updated in $QPGW_0$, the band gap consistently increases by 0.3–0.4 eV, overestimating the energy gap with MARE of 5.66%.

TABLE I. The quasiparticle band gaps (in eV) of the post-TMOs shown in Fig. 3. The values in parentheses are obtained by $GW_0 + U_d$ calculations.

	GGA + U	G_0W_0	GW_0	$QPGW_0$	G_0W_0 @HSE06	Expt.
ZnO	1.68	2.74 (2.95)	2.97 (3.24)	3.39 (3.70)	3.22	3.44[a]
Ga_2O_3	2.71	4.62	4.96	5.23	5.30	4.90[b]
In_2O_3	1.51	2.60	2.80	3.14	3.35	2.90[c]
SnO_2	1.30	3.10	3.43	3.78	3.89	3.56[d]

[a]Reference [6].
[b]Reference [38].
[c]Reference [20].
[d]Reference [17].

We also applied G_0W_0 on top of hybrid functional results (denoted as G_0W_0@HSE06) as the recipe has been frequently adopted in literature [17–20]. Interestingly, the G_0W_0@HSE06 results are very similar to $QPGW_0$ results. We note that G_0W_0@HSE06 results show band gaps of SnO_2 and In_2O_3 larger by ∼200 meV than those in Refs. [17] (SnO_2) and [20] (In_2O_3), which employed G_0W_0@HSE03. This is because the smaller screening parameter in HSE06 ($\omega = 0.2$ a.u.$^{-1}$) results in the larger band gap and smaller macroscopic dielectric constant than those obtained by the HSE03 ($\omega = 0.3$ a.u.$^{-1}$) functional.

For ZnO, there exist several GW calculations with various levels of self-consistency [6,24,26–28]. Some of these studies computed on the metastable zinc-blende ZnO because of the computational convenience from the high symmetry. However, the results should be comparable to the present study because the electronic structures of zinc-blende and wurtzite ZnO are very similar [41,42]. It is noted that the band gaps of 2.97 eV (GW_0) and 3.39 eV ($QPGW_0$) in the present study show significant improvements in comparison with 2.5 eV (GW_0@GGA) and 3.0 eV ($QPGW_0$@GGA) in Ref. [6]. This is because GGA + U reduces the p-d repulsion, resulting in a better dielectric constant than GGA. The GW@GGA calculation in Ref. [24] yielded a band gap of 3.2 eV as the large dielectric constant from GGA (see Fig. 2) is adjusted during the iteration in W. In the case of fully self-consistent $QPGW$@GGA calculation, the band gap of ZnO was ∼3.8 eV that overestimates the experimental band gap of 3.44 eV due to the underestimated dielectric constant [6,26,27].

In the above, it was mentioned that the optical dielectric constant critically affects the quasiparticle energy gap. To demonstrate this explicitly, we show in Fig. 4 the converged band gap from GW_0 with respect to $\varepsilon^{\infty}_{\mathrm{RPA}}$ obtained by the starting DFT functional. The magnitude of $\varepsilon^{\infty}_{\mathrm{RPA}}$ is always of the order of HSE06, GGA + U, and GGA as shown in Fig. 2. In Fig. 4 the inverse relation between the band gap and $\varepsilon^{\infty}_{\mathrm{RPA}}$ is confirmed in every post-TMO. The band gap can vary up to 0.8 eV depending on the choice of the functional, which underscores the importance of correct dielectric constant.

We have chosen W_0 rather than self-consistent W on the basis of the dielectric constant. One may question whether this is affected if the band gap is adopted as the criteria for determining the level of self-consistency. To examine this, we carried out the GW and $QPGW$ calculations on ZnO and SnO_2 with initial GGA ground states. The band gaps of GW($QPGW$) are found to be 3.13(3.90) and 3.82(4.41) eV for ZnO and SnO_2, respectively. Therefore, the $QPGW$ and GW band gaps (except for the GW band gap of ZnO) are overestimated in comparison with the experimental values, which is consistent with other sp materials [26–28]. Even though the GW band gap of ZnO is closer to the experimental value than for GW_0 in Table I, the Zn-d level is still underbound by ∼1 eV implying that significant p-d repulsion remains. This concludes that updating W is not recommended in post-TMOs.

B. Change in quasiparticle level and wave functions

In Fig. 5 we display quasiparticle shifts with respect to GGA + U eigenvalues. The valence band of post-TMOs can be divided into three subbands according to their main orbital characters; O-s, O-p, and metal-d. In most cases, the quasiparticle shift in each subband is well approximated as linear lines. Such relations between GW and DFT energy levels were also noted in other materials [43–45]. Figure 5 indicates that the band gap widening is largely attributed to the upshift of conduction bands, although the downshifts of valence bands are also substantial, particularly in ZnO and SnO_2.

It is also seen in Fig. 5, the amount of the shift for d level is relatively small compared to other subbands in spite of its localized nature. This is because the energy position of metal-d bands was already corrected through U_{eff} terms. We also present the quasiparticle shifts in $QPGW_0$ as filled disks and it is found that the update of wave functions in $QPGW_0$ rigidly lower the energy levels with respect to GW_0

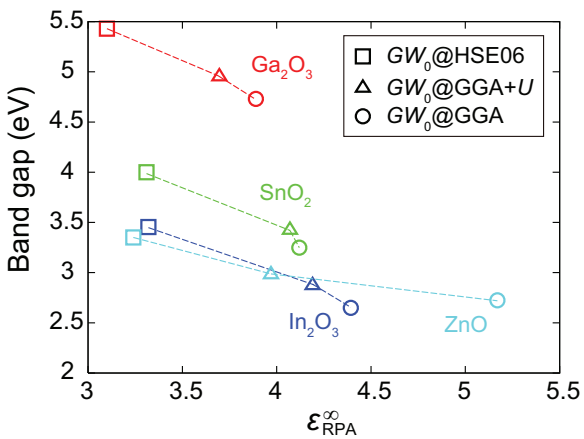

FIG. 4. (Color online) The GW_0 band gap obtained with different starting functionals (GGA, GGA+U, and HSE06) represented as an optical dielectric constant in the abscissa.

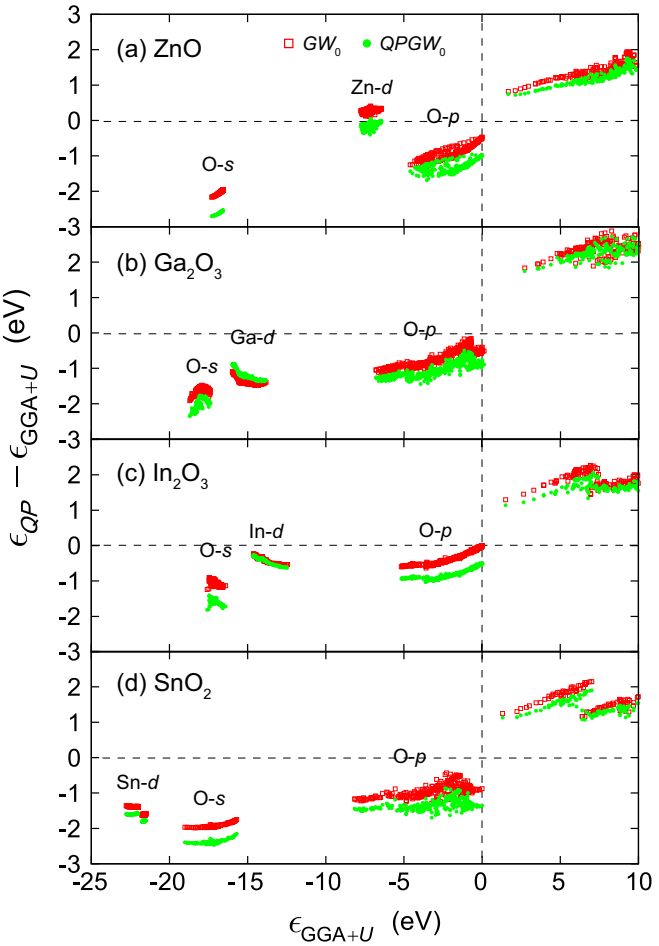

FIG. 5. (Color online) Quasiparticle shifts with respect to the GGA + U eigenvalues. The dashed vertical line indicates the Fermi level.

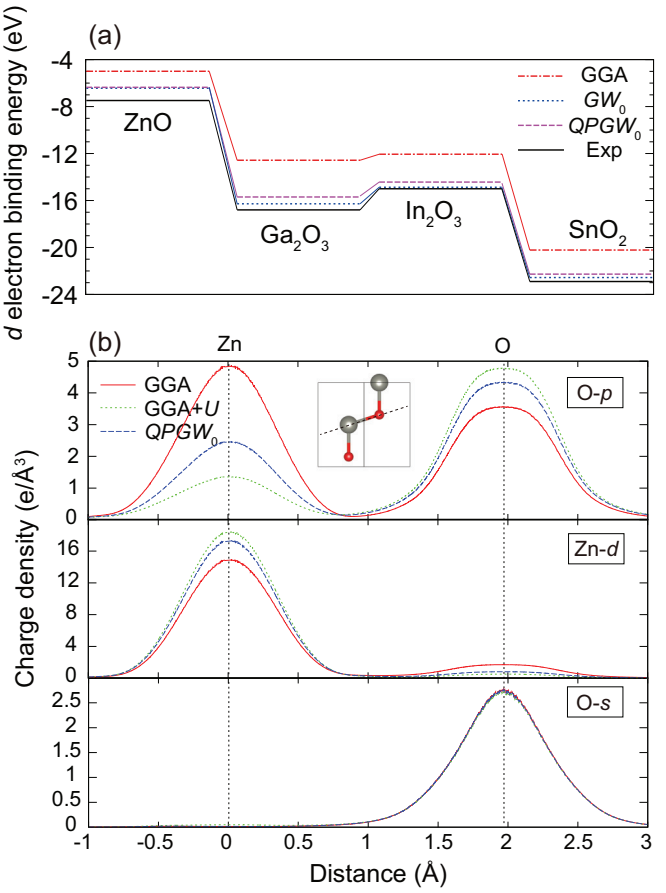

FIG. 6. (Color online) (a) The metal-d band position with respect to the valence top. The reference experimental values are 7.5, 16.8, 15.0, and 22.9 eV for ZnO [25], Ga_2O_3 [47], In_2O_3 [48], and SnO_2 [49] measured from x-ray absorption spectroscopy (XAS) or angle-resolved photoemission spectroscopy (ARPES). (b) The line profile of charge density in ZnO along the line shown in the inset.

values. In particular, the valence band shifts down further than the conduction band, which results in the larger gaps when the wave functions are updated. The origin of this can be explained below in terms of the change in charge densities.

Figure 6(a) displays the position of the computed d-band center referenced to the valence band maximum (VBM). The d-level positions in the GGA + U method were fitted to the experimental data, and so they are omitted in the figure. It is found that the GGA functional consistently yields too shallow d levels, roughly 3–4 eV above the experimental measurements. The shallow d level results in a strong hybridization with oxygen p bands, which in turn reduces the band gap through p-d repulsion. The shallow d level mainly originates from the strong self-interaction within the conventional DFT calculations. This is cured in the GW approximation and the d-band centers are much closer to the reference positions. However, the d-electron binding energy is still higher than experiment, particularly for ZnO, which is consistent with previous GW studies [6,28]. Such underbinding of d electrons was not fully corrected even in the self-consistent $QPGW$ calculation considering the vertex correction [6]. This might be because the GW method is not completely free of self-interaction [46].

To examine how the wave function changes in $QPGW_0$, in Fig. 6(b), we plot the partial electron density of each subband in valence along the Zn-O bond within GGA, GGA + U, and $QPGW_0$. (GW_0 calculation maintains the wave function obtained with GGA + U.) It is noted that pseudowave functions are used in Fig. 6(b) and so the nodal structures are incorrect inside the core region. The electron density of the O-p subband in GGA is significantly hybridized with Zn-d due to the shallow nature of the Zn-d band. In contrast, GGA + U and $QPGW_0$ reduce the hybridization between Zn-d and O-p bands by energetically separating them. It can also be observed that the hybridization in $QPGW_0$ lies in between GGA and GGA + U, and this is consistent with the d-band position shown in Fig. 6(a). While the degree of hybridization changes with functionals, we find that the orbital shapes are nearly identical, as can be seen with the O-s subband in the bottom figure of Fig. 6(b). We also find that the orbital hybridization is changed for other post-TMOs, although the variation is less dramatic than ZnO.

In the above, $QPGW_0$ consistently yielded larger band gaps in comparison with those of GW_0. It was also reported that the $QPGW_0$ calculation for sp-based oxide and nitride materials tends to yield larger band gap than the GW_0

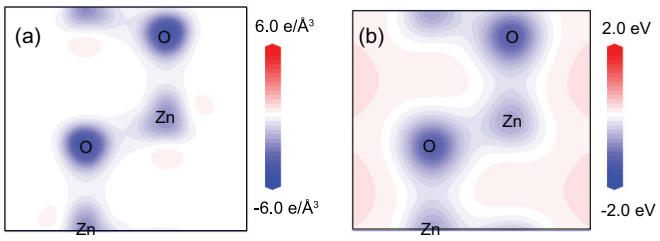

FIG. 7. (Color online) Differences in (a) electron density and (b) local potential difference $QPGW_0$ and GGA + U.

calculation [6]. To reveal the origin of that, we plot the difference in the electron density of ZnO between $QPGW_0$ and GGA + U (since the wave functions in GW_0 are same with those in GGA + U) as shown in Fig. 7(a). It is found that the electron density near O sites is significantly reduced while it is slightly increased in the interstitial sites. (Such change in the electron density commonly appears in other post-TMOs.) This variation of the charge density reduces the electron-electron repulsive interaction near atomic sites, and thus, the electrostatic potential becomes more attractive near those locations, especially at O sites, as shown in Fig. 7(b). This may explain why $\varepsilon_{\mathrm{QP}} - \varepsilon_{\mathrm{GGA}+U}$ is more negatively shifted for orbitals at O sites (valence) than those at cation sites (conduction) in Fig. 5, which results in additional gap opening in $QPGW_0$ calculation.

C. $GW_0 + U_d$ scheme

In the above, the underestimation of d-band position is the most severe for ZnO. One may question whether this is related to the outlying behavior of ZnO in the band gap trend in Fig. 3. As mentioned above, the underbinding originates from the self-interaction among the Zn-d manifold that is not fully addressed by GW. To address this, we introduce a small on-site term (U_d) of 3 eV on the Zn-d orbital within the GW_0 scheme. The value for U_d was chosen such that the d-band position in $GW_0 + U_d$ lies within 0.1 eV of the experimental data. In Fig. 3, the resulting GW_0 and $QPGW_0$ band gaps are shown as dashed triangles. It can be observed that the results among the same GW levels are now highly consistent, i.e., GW_0 shows the best results (with MARE of 3.53%) while $QPGW_0$ overestimates the gap by 7.18%. This concludes that $GW_0(+U_d)$ is the most reliable GW scheme considered in the present work. We note that in Ref. [32] the GW band gap for TMOs were improved by applying a small positive potential to d levels (occupied or unoccupied), which has the same effect on the occupied electron as the above U_d term. For other post-TMOs, we found that the application of U_d during GW_0 iteration did not influence the band gap significantly.

There has been an issue on the nature of the band gap of In_2O_3; various band gaps between 2.62 and 3.75 eV have been reported experimentally [48,50–52]. In Ref. [53] it was suggested, based on x-ray measurements and GGA + U calculations, that the fundamental band gap of undoped In_2O_3 is 2.9 eV and the band gap larger than 3.5 eV is a result of forbidden transition in optical measurements. The present work yields 2.80 eV as the best estimate of the minimum gap within GW_0, which supports Ref. [53].

D. scCOHSEX + G_0W_0 method

Until now, we compared various levels of self-consistent GW_0 schemes. There is an alternative GW approach in which the static screening based on the self-consistent Coulomb-hole plus screened-exchange (scCOHSEX) is used to update the eigenfunctions and eigenvalues first, and then one-shot G_0W_0 with full frequency dependence is carried out (scCOHSEX + G_0W_0) [54]. This was originally proposed to efficiently obtain results close to $QPGW$ because it mainly relies on the static screening instead of the dynamic one. We apply scCOHSEX(+G_0W_0) on ZnO and SnO_2 and it is found that the scCOHSEX(+G_0W_0) band gaps of ZnO and SnO_2 are 4.59 (4.60) and 4.96 (4.88) eV, respectively, which are larger than the experimental values of ZnO (3.44 eV) and SnO_2 (3.56 eV), leading to the overestimation of ∼35%. Similar overestimation in the band gap was reported in Ref. [54] in the case of Si; the band gap of scCOHSEX + G_0W_0 was 1.56 eV which is larger than $QPGW$ (1.47 eV) and experimental (1.14 eV) values.

E. Influence of pseudopotential type

Recently, there have been discussions on how the pseudization scheme used in constructing pseudopotentials influence GW results. Foremost, some GW studies based on norm-conserving pseudopotential argued that 3s and 3p electrons for ZnO and Ga_2O_3 (or 4s and 4p electrons for In_2O_3 and SnO_2) should be treated as the valence electrons as they share the shell with a d electron [23,55]. The present GW implementation within VASP approximately considers the core-valence interaction at the Hartree-Fock level, which allows us to keep the s and p electrons in the core without compromising the accuracy significantly [28,29]. To examine the core effect more explicitly, we compared the G_0W_0@GGA gap of ZnO using Zn^{12+} ($3d^{10}4s^2$ for valence) and Zn^{20+} ($3s^23p^63d^{10}4s^2$ for valence) PAW pseudopotentials. Here the +U scheme is avoided since the empirical parameter U_{eff} influences the result differently depending ont the pseudopotential type. It was found that the discrepancy between the results from the two pseudopotentials is ∼10 meV, confirming that the core-valence interaction is well addressed in the code.

In addition, the PAW potentials were recently introduced with better scattering properties at high energies, which might be crucial when a large number of the empty bands are used to evaluate the self-energy [29]. To examine the effect of this improvement in the pseudopotential, we compared G_0W_0@GGA results on ZnO and SnO_2 from the conventional PAW potential and those with improved scattering properties, and found that the results agree within ∼60 meV. Therefore, it is unlikely that any significant change will result with the newly introduced PAW potentials.

To further confirm the validity of using pseudopotential-based plane-wave approach, we compare the energy levels of ZnO with all-electron (AE) results in Ref. [56] calculated by using a linearized augmented-plane-wave (LAPW) basis set. Since these AE results were obtained with G_0W_0 on LDA wave functions, we reproduce the VASP results with the same computational condition for the fair comparison(Table II). It is seen that the LDA results agree within 0.1 eV. For the quasiparticle energies, the maximum difference increases to ∼0.2 eV but the band gap agrees within 0.06 eV. In addition,

TABLE II. The LDA and G_0W_0 energies (in eV) of ZnO at Γ point are provided with respect to the valence band maximum. The first column indicates the main orbital character of each band. G_0W_0 is applied to LDA ground states perturbatively. All-electron results [56] obtained by using linearized augmented-plane-wave (LAPW) are shown for comparison and Δ is the difference between the energies of PAW and LAPW.

		LDA			G_0W_0		
Char.	Band	PAW	LAPW	Δ	PAW	LAPW	Δ
O-s	1	−17.81	−17.84	−0.03	−18.44	−18.56	−0.12
	2	−17.03	−17.06	−0.03	−17.75	−17.78	−0.03
Zn-d	3, 4	−5.78	−5.80	−0.02	−6.42	−6.62	−0.20
	5	−5.71	−5.74	−0.03	−6.38	−6.58	−0.20
	6, 7	−5.69	−5.62	0.07	−6.25	−6.46	−0.21
	8	−5.59	−5.53	0.06	−5.73	−5.90	−0.17
	9, 10	−4.60	−4.70	−0.10	−5.62	−5.68	−0.06
	11, 12	−4.39	−4.48	−0.09	−5.42	−5.65	−0.23
O-p	13	−4.09	−4.19	−0.10	−5.00	−5.20	−0.20
	14, 15	−0.81	−0.74	0.07	−0.89	−0.84	0.05
	16	−0.08	−0.10	−0.02	−0.05	−0.08	−0.03
	17, 18	0.00	0.00	0.00	0.00	0.00	0.00
Zn-s	19	0.74	0.78	0.03	2.38	2.44	0.06
	20	5.07	5.12	0.06	7.11	7.25	0.08

the AE band gaps from $QPGW$ calculations were reported to be of 3.87 eV in Refs. [26,27]. We carried out the same types of $QPGW$ calculations and obtained 3.90 eV which agrees well with the AE results. Therefore, it is confirmed that the present approach using PAW pseudopotentials produces the band gap close to AE calculations.

F. Compound structure

So far we focused on the binary post-TMOs, and it was found that $GW_0(+U_d)$ calculation with GGA + U ground states yielded the most reliable band gaps. As another test, we compute on the compound structure of post-TMOs, specifically crystalline $InGaZnO_4$, which is receiving recent attention owing to its application to transparent field effect transistors [1,57]. The structural information from experiment is used and three formula units are included within the unit cell (21 atoms in total) [1,57]. For the quasiparticle band gap of $InGaZnO_4$, we apply GW_0 calculation with GGA + U ground state and additional U_d on Zn as in the foregoing subsections. We employed 288 bands and $7 \times 7 \times 1$ **k**-point mesh grid to evaluate the self-energy. It is found that the quasiparticle band gap is 3.74 eV that is in good agreement with the experimental value of 3.7 eV, which was measured by the optical absorption measurement [57]. This supports that the $GW_0(+U_d)$ can be reliably transferable to various structures of post-TMOs.

IV. CONCLUSION

In summary, we investigated the electronic structure of binary as well as quaternary post-TMOs within GW approximations. Various levels of self-consistency and starting functionals were tested and it was found that the GW_0 scheme with GGA + U as the DFT functional turned out to give best results in every aspect of band structure. Nevertheless, the computation with ZnO still suffers from the shallow d band and we proposed a modified scheme, $GW_0 + U_d$, which significantly improved the band gap. On the other hand, $QPGW_0$, the highest level of self-consistency in the present work, was found to overestimate the band gap. By establishing the proper GW scheme, we believe that the present work will serve as a useful guide for accurately estimating the band gap of post-TMOs and their compound structures.

ACKNOWLEDGMENTS

This work was supported by the Pioneer Research Center Program through the National Research Foundation of Korea funded by the Ministry of Education, Science and Technology (2012-0009563). The computations were carried out at KISTI (No. KSC-2013-C3-011).

[1] K. Nomura, H. Ohta, K. Ueda, T. Kamiya, M. Hirano, and H. Hosono, Science **300**, 1269 (2003).
[2] K. Nomura, H. Ohta, A. Takagi, T. Kamiya, M. Hirano, and H. Hosono, Nature (London) **432**, 488 (2004).
[3] Y. Kang, S. H. Jeon, Y. W. Son, Y. S. Lee, M. Ryu, S. Lee, and S. Han, Phys. Rev. Lett. **108**, 196404 (2012).
[4] P. Erhart, K. Albe, and A. Klein, Phys. Rev. B **73**, 205203 (2006).
[5] A. Janotti and C. G. Van de Walle, Phys. Rev. B **76**, 165202 (2007).
[6] M. Shishkin, M. Marsman, and G. Kresse, Phys. Rev. Lett. **99**, 246403 (2007).
[7] K. Yamaguchi, Solid State Chem. **131**, 739 (2004).
[8] K. G. Godinho, A. Walsh, and G. W. Watson, J. Phys. Chem. C **113**, 439 (2009).
[9] S. Park, B. Lee, S. H. Jeon, and S. Han, Curr. Appl. Phys. **11**, S337 (2011).
[10] Y. Kang, H. Song, H.-H. Nahm, S. H. Jeon, Y. Cho, and S. Han, APL Mater. **2**, 032108 (2014).
[11] A. Alkauskas and A. Pasquarello, Phys. Rev. B **84**, 125206 (2011).
[12] H. K. Noh, K. J. Chang, B. Ryu, and W. J. Lee, Phys. Rev. B **84**, 115205 (2011).
[13] A. Janotti and C. G. Van de Walle, Appl. Phys. Lett. **87**, 122102 (2005).
[14] A. K. Singh, A. Janotti, M. Scheffler, and C. G. Van de Walle, Phys. Rev. Lett. **101**, 055502 (2008).
[15] F. Oba, A. Togo, I. Tanaka, J. Paier, and G. Kresse, Phys. Rev. B **77**, 245202 (2008).
[16] J. B. Varley, A. Janotti, C. Franchini, and C. G. Van de Walle, Phys. Rev. B **85**, 081109 (2012).
[17] A. Schleife, J. B. Varley, F. Fuchs, C. Rödl, F. Bechstedt, P. Rinke, A. Janotti, and C. G. Van de Walle, Phys. Rev. B **83**, 035116 (2011).

[18] A. Schleife, F. Fuchs, C. Rödl, J. Furthmüller, and F. Bechstedt, Phys. Status Solidi B **246**, 2150 (2009).
[19] B. Höffling, A. Schleife, C. Rödl, and F. Bechstedt, Phys. Rev. B **85**, 035305 (2012).
[20] F. Fuchs and F. Bechstedt, Phys. Rev. B **77**, 155107 (2008).
[21] P. D. C. King, T. D. Veal, A. Schleife, J. Zuniga-Perez, B. Martel, P. H. Jefferson, F. Fuchs, V. Munoz-Sanjose, F. Bechstedt, and C. F. McConville, Phys. Rev. B **79**, 205205 (2009).
[22] B.-C. Shih, Y. Xue, P. Zhang, M. L. Cohen, and S. G. Louie, Phys. Rev. Lett. **105**, 146401 (2010).
[23] H. Dixit, R. Saniz, D. Lamoen, and B. Partoens, J. Phys.: Condens. Matter **22**, 125505 (2010).
[24] S. Lany and A. Zunger, Phys. Rev. B **81**, 113201 (2010).
[25] L. Y. Lim, S. Lany, Y. J. Chang, E. Rotenberg, A. Zunger, and M. F. Toney, Phys. Rev. B **86**, 235113 (2012).
[26] M. van Schilfgaarde, T. Kotani, and S. Faleev, Phys. Rev. Lett. **96**, 226402 (2006).
[27] T. Kotani, M. van Schilfgaarde, and S. V. Faleev, Phys. Rev. B **76**, 165106 (2007).
[28] M. Shishkin and G. Kresse, Phys. Rev. B **75**, 235102 (2007).
[29] M. Shishkin and G. Kresse, Phys. Rev. B **74**, 035101 (2006).
[30] G. Kresse and J. Furthmuller, Phys. Rev. B **54**, 11169 (1996); P. E. Blöchl, *ibid.* **50**, 17953 (1994).
[31] G. Kresse and D. Joubert, Phys. Rev. B **59**, 1758 (1999).
[32] S. Lany, Phys. Rev. B **87**, 085112 (2013).
[33] J. P. Perdew, K. Burke, and M. Ernzerhof, Phys. Rev. Lett. **77**, 3865 (1996).
[34] S. L. Dudarev, G. A. Botton, S. Y. Savrasov, C. J. Humphreys, and A. P. Sutton, Phys. Rev. B **57**, 1505 (1998).
[35] J. Heyd, G. E. Scuseria, and M. Ernzerhof, J. Chem. Phys. **118**, 8207 (2003).
[36] H. He, R. Orlando, M. A. Blanco, R. Pandey, E. Amzallag, I. Baraille, and M. Rérat, Phys. Rev. B **74**, 195123 (2006).
[37] N. Ashkenov, B. N. Mbenkum, C. Bundesmann, V. Riede, M. Lorenz, D. Spemann, E. M. Kaidashev, A. Kasic, M. Schubert, G. Wagner, H. Neumann, V. Darakchieva, H. Arwin, and B. Monemar, J. Appl. Phys. **93**, 126 (2003).
[38] M. Rebien, W. Henrion, M. Hong, J. P. Mannaerts, and M. Fleischer, Appl. Phys. Lett. **81**, 250 (2002).
[39] Ü. Özgür, Y. I. Alivov, C. Liu, A. Teke, M. A. Reshchikov, S. Doğan, V. Avrutin, S.-J. Cho, and H. Morkoç, J. Appl. Phys. **98**, 041301 (2005).
[40] K. Reimann and M. Steube, Solid State Commun. **105**, 649 (1998).
[41] A. Ashrafi and C. Jagadish, J. Appl. Phys. **102**, 071101 (2007).
[42] A. Schleife, F. Fuchs, J. Furthmüller, and F. Bechstedt, Phys. Rev. B **73**, 245212 (2006).
[43] S. Sharifzadeh, A. Biller, L. Kronik, and J. B. Neaton, Phys. Rev. B **85**, 125307 (2012).
[44] M. Rohlfing and S. G. Louie, Phys. Rev. B **62**, 4927 (2000).
[45] T. Körzdörfer and S. Kümmel, Phys. Rev. B **82**, 155206 (2010).
[46] W. Nelson, P. Bokes, P. Rinke, and R. W. Godby, Phys. Rev. A **75**, 032505 (2007).
[47] M. Michling and D. Schmeißer, IOP Conf. Series: Mater. Sci. Eng. **34**, 012002 (2012).
[48] A. Klein, Appl. Phys. Lett. **77**, 2009 (2000).
[49] M. Sinner-Hettenbach, M. Göthelid, T. Weiß, N. Barsan, U. Weimar, H. von Schenck, L. Giovanelli, and G. Le Lay, Surf. Sci. **499**, 85 (2002).
[50] P. Erhart, A. Klein, R. G. Egdell, and K. Albe, Phys. Rev. B **75**, 153205 (2007).
[51] C. McGuinness, C. B. Stagarescu, P. J. Ryan, J. E. Downes, D. Fu, K. E. Smith, and R. G. Egdell, Phys. Rev. B **68**, 165104 (2003).
[52] R. L. Weiher and R. P. Ley, J. Appl. Phys. **37**, 299 (1966).
[53] A. Walsh, J. L. F. Da Silva, S. H. Wei, C. Körber, A. Klein, L. F. J. Piper, A. DeMasi, K. E. Smith, G. Panaccione, P. Torelli, D. J. Payne, A. Bourlange, and R. G. Egdell, Phys. Rev. Lett. **100**, 167402 (2008).
[54] F. Bruneval, N. Vast, and L. Reining, Phys. Rev. B **74**, 045102 (2006).
[55] R. Saniz, H. Dixit, D. Lamoen, and B. Partoens, Appl. Phys. Lett. **97**, 261901 (2010).
[56] M. Usuda, N. Hamada, T. Kotani, and M. van Schilfgaarde, Phys. Rev. B **66**, 125101 (2002).
[57] T. Kamiya, K. Nomura, and H. Hosono, J. Disp. Technol. **5**, 273 (2009).